

Carbon Nanotubes Synthesized by CCVD Method using Diatomite and Shungite Minerals

M. Nazhipkyzy^{1,2*}, P.J.F. Harris³, A. Nurgain^{1,2}, R.R. Nemkayeva⁴

¹Institute of Combustion Problems, 172 Bogenbai Batyr str., Almaty, Kazakhstan

²Al-Farabi Kazakh National University, 71 Al-Farabi ave., Almaty, Kazakhstan

³University of Reading, Whiteknights, Reading RG6 6AF, UK

⁴National Nanotechnology Laboratory of Open Type, Al-Farabi Kazakh National University, Almaty, Kazakhstan

Article info

Received:
15 May 2021

Received in revised form:
28 July 2021

Accepted:
13 September 2021

Keywords:

Catalytic vapour deposition,
Diatomite, shungite,
Carbon nanotubes.

Abstract

In this work, carbon nanotubes were prepared using catalysts consisting of nickel particles supported on the naturally occurring minerals diatomite and shungite. The carbon source for the chemical catalytic vapour deposition (CCVD) synthesis was a propane-butane gas mixture. The synthesized multiwall carbon nanotubes (MWCNT) were characterized using Raman spectroscopy, transmission and scanning electron microscopy, and the effect of temperature on their structure was investigated. The carbon content was determined by thermogravimetric analysis. In Raman spectra of CNTs the intensity ratio $I_{(G)}/I_{(D)}$ for 650 °C is higher than that for 700 °C and then it begins to increase with increasing temperature. The results show that the diameter of CNTs which were synthesized on the surface of diatomite/shungite samples were in the range of 33–100.3 nm. The development of new methods for creating catalytic systems that allow controlling the structure of carbon particles is an important task leading to the improvement of existing approaches to the synthesis of CNTs with certain functional properties.

1. Introduction

Carbon nanotubes (CNTs) were discovered by Iijima in 1991 [1] and they continue to be the subject of close attention because of their amazing mechanical, electrical, thermal and optical properties, as well as their potential impact on wide areas of science and technology. The strength of carbon nanotubes is 50–100 times higher than steel, and the density is six times less. Guo et al. synthesized CNTs from carbonaceous gas by laser ablation method in 1994 [2]. Although they produce high-quality nanotubes both the arc discharge and the laser ablation were not widely used due to the relatively sophisticated equipment required, and the fact that these are “batch” rather than continuous processes. The third method used by Endo et al. in 1993 for obtaining CNTs [3] is chemical vapour deposition (CVD). Until now, CVD has been a prevalent method for the synthesis of CNTs [4].

Currently, the method of chemical vapor deposition has found wide application for the production of nanocrystalline films and powders. The CVD method also makes it possible to synthesize nanotubes in defined patterns by employing arrays of ordered catalyst particles on a substrate. Other advantages of the CVD method are the relatively low temperatures necessary for the growth of nanotubes, as well as good “scalability”, i.e. for large-scale production of CNTs [5]. It is known that the chemical vapor deposition method is based on the thermal decomposition of carbon-containing compounds in the presence of a catalyst. The most commonly used catalysts are nanoparticles of transition metals (Fe, Co, Ni, Mo, and mixtures thereof). A metal nanoparticle acts as a catalytic center for the growth of a carbon nanotube. The particle size of the catalyst is one of the factors determining the diameter of the synthesized CNTs. For the growth of CNTs, a variety of carbon-containing gases and liquids are used that undergo pyrolysis at synthesis temperatures (500–1200 °C). Examples of such

*Corresponding author. E-mail: meruert82@mail.ru

precursors are CH_4 , CO , C_2H_2 , C_2H_4 , C_6H_6 , C_6H_{12} and other hydrocarbons. Many studies show that catalyst and reaction temperature are important factors which affect the yield of CNTs [5–13]. In this paper, the synthesis of carbon nanotubes using nickel catalysts supported on the naturally occurring minerals diatomite and shungite is described. Diatomite and shungite were chosen as a matrix due to their low cost.

2. Experimental part

2.1. Material preparation

Carbon nanotubes were synthesized by CCVD method. Figure 1 presents the schematic image of CCVD setup. Propane-butane mixture was used as a carbon-containing gas, and shungite/diatomite was used as a catalyst carrier. A sample of shungite/diatomite was first saturated with an alcoholic solution of nickel nitrate, then it was dried.

This system consists of a furnace with a quartz reaction tube of 35 mm in diameter and 450 cm in length. The central part of the reactor can be heated to 1000 °C. The measurement of temperature was made using a chromel-alumel thermocouple. The process of growth was carried out by catalytic decomposition of a propane-butane gas mixture on a shungite/diatomite substrate with a previously prepared catalyst.

High purity propane-butane gas mixture (flow rate of 80–100 ml/min) was selected as carbon source. High purity Ar was as the inert gas. Nickel salt has obvious catalysis effect, so nickel(II) nitrate was as the catalyst for synthesis of CNTs. Shungite/diatomite with nickel(II) nitrate were heated at 400–500 °C for optimizing of catalyst particles. The reaction mixture containing a source of hydrocarbon and inert gas is passed through a catalyst bed at temperatures in the range from 650 to 800 °C. Then the system is cooled to room temperature.

2.2. Material characterization

Raman spectroscopy NTegra Spectra (NT-MDT, Russia) was used to structurally characterize the CNTs. Scanning electron microscopy (SEM: FEI Quanta) and high resolution transmission electron microscope (HRTEM: JEOL JEM-2100) was used to image the morphology and the structure of the grown material. The carbon content was determined by thermogravimetric (TGA) analysis (TA TGAQ50).

3. Results and discussions

The Raman spectra of MWCNT in the case of both diatomite (Fig. 2) and shungite (Fig. 3) substrates show the four characteristic peaks: the D band at about 1360 cm^{-1} , the G band at 1580 cm^{-1} , the 2D (G') band at 2710 cm^{-1} and D+G band (also assigned as D+D') at about 2930 cm^{-1} . The D band indicates the presence of defects in the MWCNT sample, like carbon impurities with sp^3 bonding or dangling sp^2 bonds at the edges. The G band is due to sp^2 graphitic nature of the sample and its FWHM can indicate the crystallinity of the sample. The 2D band is associated with the long-range order in a sample mainly along the crystallographic c-axis and also provides information on the number of walls.

The 2D peak arises from the two-phonon, second order scattering process that results in the creation of an inelastic phonon [14], no defects are required for its activation. While D+G band is the combination of phonons with different momenta and thus requires a defect for its activation [15].

Despite some ambiguities in Raman spectra of the samples obtained at higher temperatures, there is a certain correlation between the quality of CNTs and the synthesis temperature. The data FWHM of the G peak demonstrate that the crystallinity of CNTs increases with increasing reaction temperature (Fig. 3). Moreover, it should be noticed

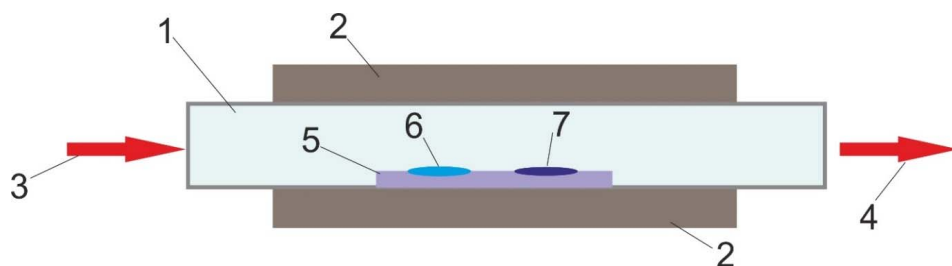


Fig. 1. A scheme of CCVD setup: 1 – quartz tube; 2 – furnace; 3 – gas inlet; 4 – gas outlet; 5 – porcelain boat; 6 – CNTs; 7 – catalysts.

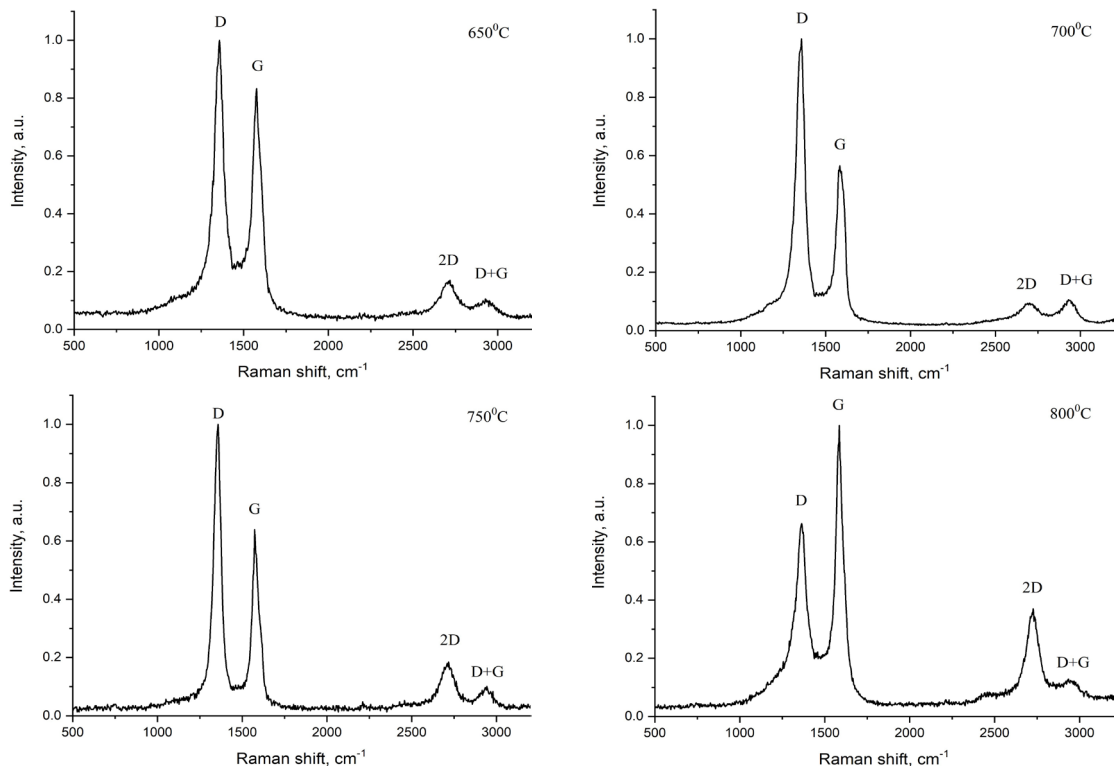


Fig. 2. Raman spectra of MWCNT synthesized on diatomite at different temperatures.

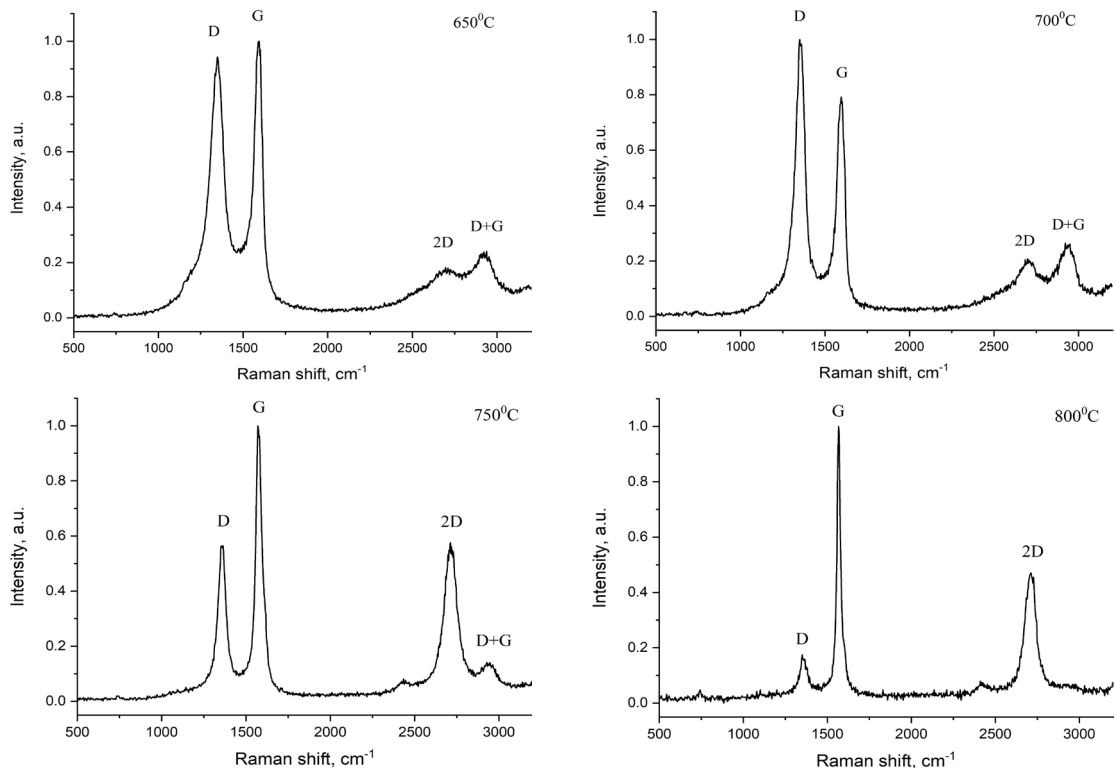


Fig. 3. Raman spectra of MWCNT synthesized on shungite at different temperatures.

that samples on shungite substrate demonstrate lower values of G peak width and i.e. the highest crystallinity of the structure.

The intensity ratio $I_{(G)}/I_{(D)}$ is known to be directly proportional to the graphitization degree of

carbon materials. Thus, using this value, one can characterize the level of disorder in CNT samples. As disorder in MWCNT changes, $I_{(G)}/I_{(D)}$ displays 2 types of behavior. The first type of “low” defect density is characterized by decrease of the ratio

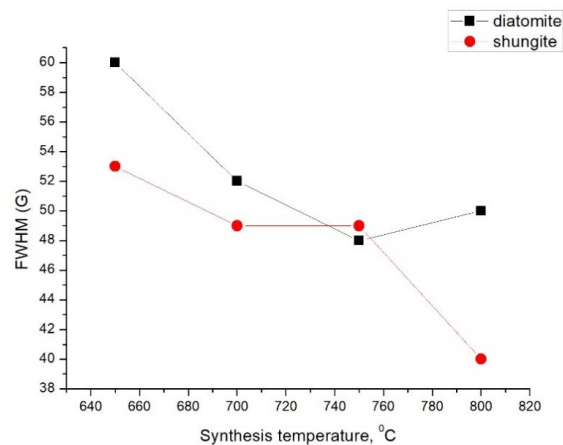


Fig. 4. Dependence of crystallinity of CNT samples on synthesis temperature.

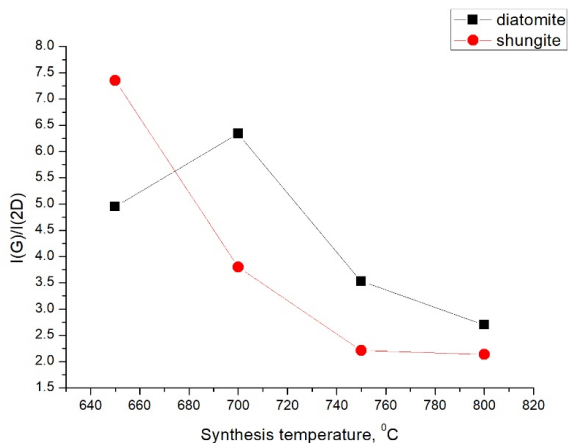


Fig. 6. Ratios of G and 2D Raman peaks intensity for different synthesis temperatures.

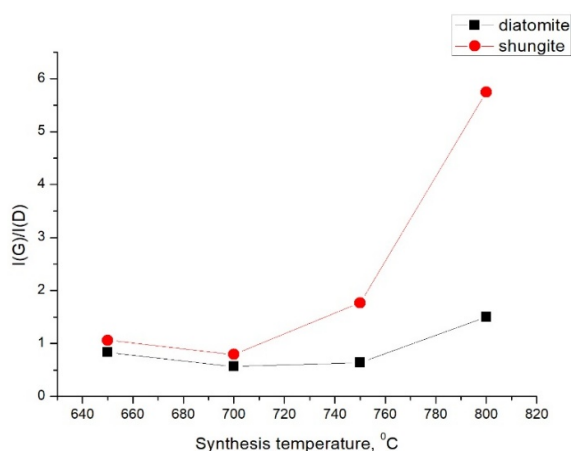


Fig. 5. The evolution of $I_{(G)}/I_{(D)}$ ratio with the synthesis temperature.

with increasing defect density. When the amount of defects reaches a certain threshold, the “high” defect density behavior occurs, at which $I_{(G)}/I_{(D)}$ begin to increase with the increasing amount of defects, which can be observed in the case of more amorphous carbon structures [16]. In Raman spectra of CNTs the intensity ratio $I_{(G)}/I_{(D)}$ for 650 °C is higher than that for 700 °C and then it begins to increase with increasing temperature as it is shown in Fig. 5. Thus, there is a switch point at 700 °C when the “low” defect density regime became valid.

Some authors claim that $I_{(G)}/I_{(2D)}$ ratio may represent a more accurate measurement of MWCNT quality or purity [17] and, as it was stated above, the rise of 2D band indicates the increase of 3D ordering. Analysis of $I_{(G)}/I_{(2D)}$ (Fig. 6) showed that long-range order in our MWCNT samples also increases with increasing synthesis temperature, i.e. at higher temperature, the tubes have higher length without bundles.

One can notice considerably different spectrum of CNT in case of shungite substrate and synthesis temperature of 800 °C, which demonstrates extremely low values of FWHM of G peak and $I_{(G)}/I_{(D)}$ ratio. According to Nii et al. [18] this kind of Raman spectrum is observed on the sample with diameter less than 10 nm and can be attributed to SWCNTs or double-walled carbon nanotubes (DWCNTs) and not to MWCNTs.

As well as the Raman results SEM images were taken of CNT samples prepared at different temperatures (Figs. 7 and 8).

It is shown that from SEM images diameter of CNT samples on the surface of diatomite/shungite samples were in the range of 33–100 nm.

The initial diatomite, initial shungite and CNTs which were synthesized at 800 °C on the surface of diatomite/shungite substrate were investigated by TEM, as shown in Fig. 9.

From TEM images it is shown that lattice fringes of approximately 0.21 nm in the metal particles of NiO. The pure diatomite mineral was largely amorphous, but with some areas which showed lattice lines. The nanotube images show tubular structures with poor graphitization. The sample seemed to consist of amorphous material and graphite crystals.

3.1. TGA Analysis

The carbon nanotube samples grown on diatomite and shungite substrate at 800 °C were investigated by TGA. Results for CNT samples on diatomite at 800 °C are shown in Fig. 10. Results for CNT samples on shungite at 800 °C are shown in Fig. 11.

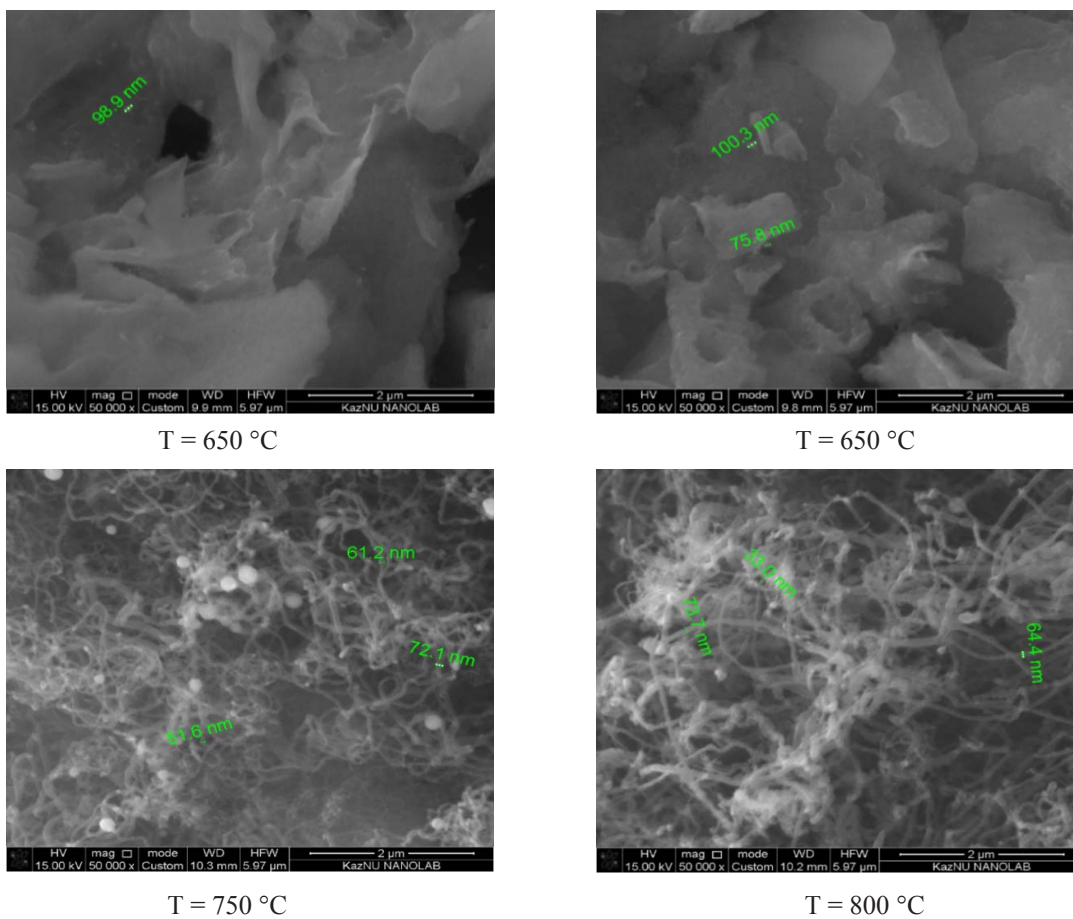


Fig. 7. SEM images of diatomite samples impregnated with a nickel salt.

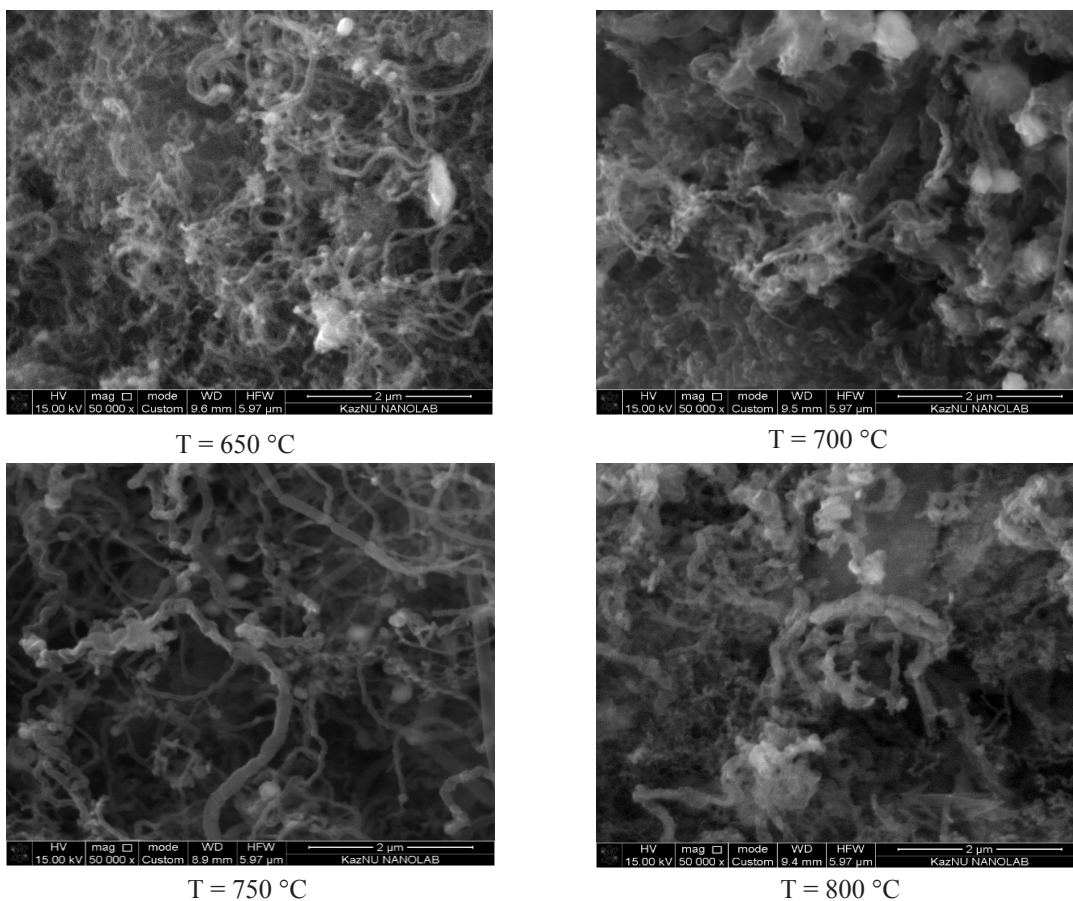


Fig. 8. SEM images of shungite samples impregnated with a nickel salt.

The carbon nanotube sample was softly ground prior to TGA analysis. Then the sample was heated in an alumina crucible with an air gas flow rate of 60 ml/min. The dynamic measurement was made from 18 to 850 °C with a ramp rate of 10 °C/min. The samples have been done in alumina pans (a second pan added on the platinum instrument pan) since they are the common ones used with air experiments. However, a run in a platinum pan (a second pan added on the platinum instrument pan) (Subtract 800 °C, run 200918) has also been done to check the reproducibility. Two runs were done and a comparison between them was also done. For the CNT samples on the diatomite sample the TGA curve decreases steadily from the start. The TGA curve (weight %, green curve) starts with two different residual weight losses named on the graph as solvent. As it happened with the analysis run in N₂, two different rates could be identified (named in the N₂ analysis as solvent A and B). These weight losses could be due to solvents or other residual compound of the sample. There is not a clear transition between both steps.

The DTA (derivative of the weight loss as a function of T, pink curve) shows two degradation peaks at 668.06 and 694.80 °C. These two peaks are not resolved. These temperatures are the points of maximum weight loss (corresponding to oxidation temperatures). The first peak starts at 610.37 °C (extrapolated onset T). The second peak is not well separated from the first peak, therefore, it was not possible to give the onset temperature. A slower temperature ramp could increase resolution and hence the separation between both peaks. The degradation process is not complete at 850 °C, with a residual mass of 39.66% (3.531 mg), being the total weight loss of the process of 60.34% (5.374 mg). These results seem similar to the results under an air atmosphere of this work [19].

For the CNT samples on the surface of shungite substrate (Run 051218, in an alumina pan) the TGA curve decreases steadily from the start. The TGA curve (weight %, green curve) starts with two different residual weight losses named on the graph as solvent. As it happened with the analysis run in N₂, two different rates could be identified

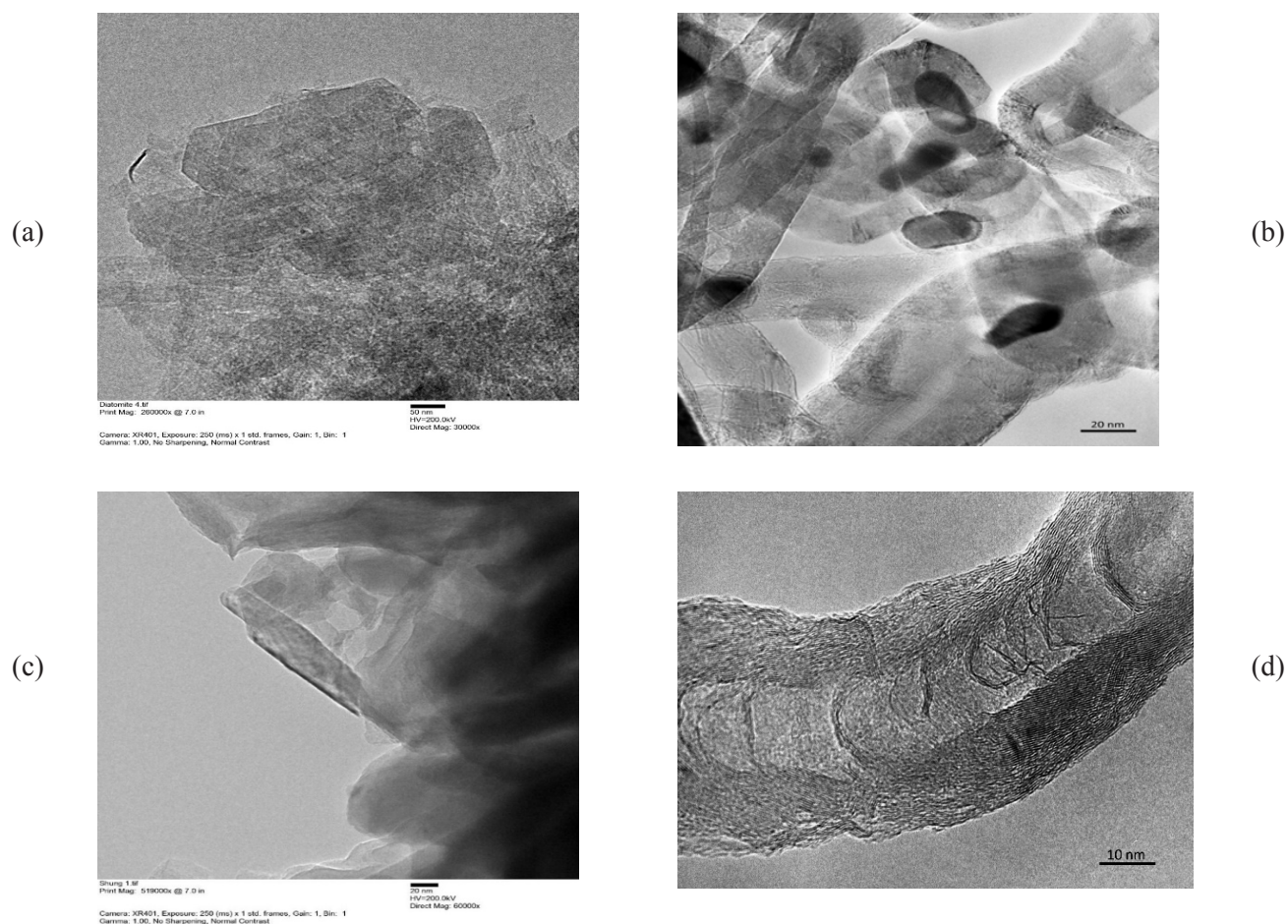


Fig. 9. TEM images of the samples: (a) – initial diatomite; (b) – CNT on the surface of diatomite samples; (c) – initial shungite, (d) – CNT on the surface of shungite samples.

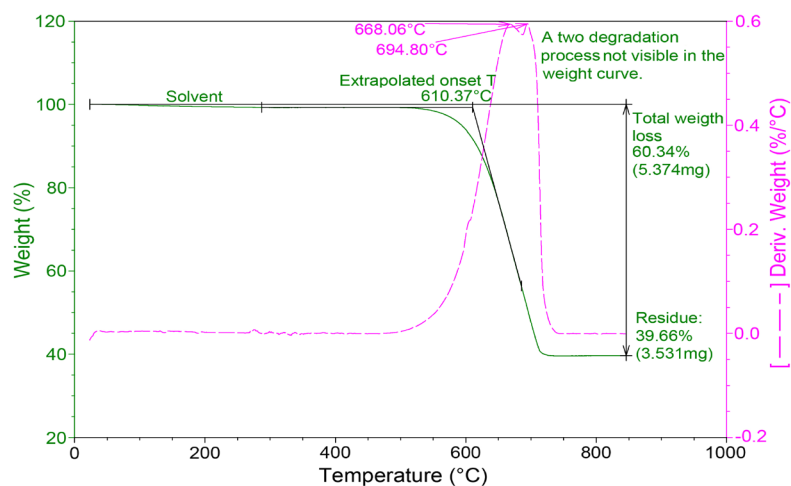


Fig. 10. TGA analysis of CNT samples on diatomite at 800 °C under air atmosphere.

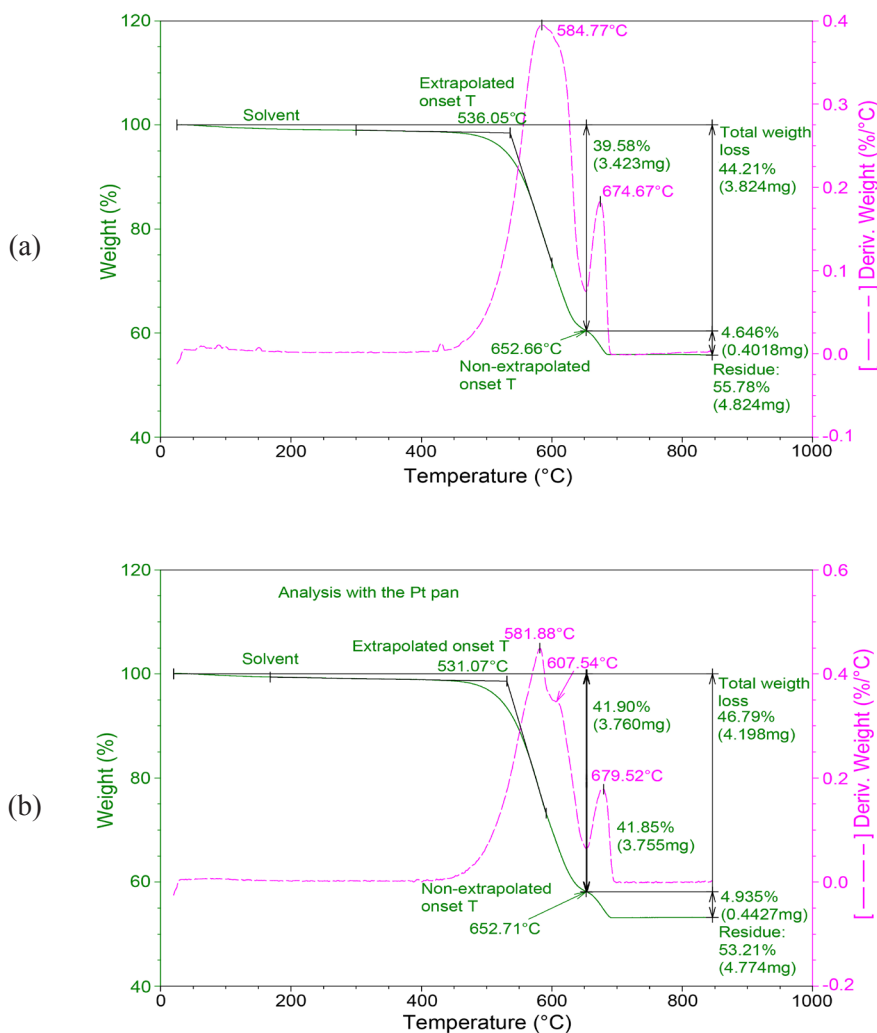


Fig. 11. TGA analysis of CNT samples on shungite at 800 °C under air atmosphere.

(named in the N_2 analysis as solvent A and B). These weight losses could be due to solvents or other residual compound of the sample. There is not a clear transition between both steps. The DTA

(derivative of the weight loss as a function of T, pink curve) shows a degradation peak at 584.77 °C and a second one at 674.67 °C (corresponding to oxidation temperatures).

These temperatures are the points of maximum weight loss. The first peak (weight loss of 39.58%, 3.423 mg, Fig. 11a) is not well resolved, a second peak seems to be appreciated, but it is less well resolved than in the Ni 800 °C diatomite sample so no DTA temperature can be given. This first peak starts at 536.05 °C (extrapolated onset T, Fig. 11a). The second visible degradation peak starts at 652.66 °C (non-extrapolated onset T, Fig. 11a), with a DTA peak at 674.67 °C and a weight loss of 4.646% (0.4018 mg, Fig. 10a). The degradation process is not complete at 850 °C, with a residual mass of 55.78% (4.824 mg), being the total weight loss of the process of 44.21% (3.824 mg, Fig. 11a). These results seem similar to the results under an air atmosphere of the work [8]. According to the run 200918 in a platinum pan, the TGA curve decreases steadily from the start.

The TGA curve (weight %, green curve) starts with two different residual weight losses named on the graph as solvent. As it happened with the analysis run in N₂, two different rates could be identified (named in the N₂ analysis as solvent A and B). These weight losses could be due to solvents or other residual compound of the sample. There is not a clear transition between both steps. The DTA (derivative of the weight loss as function of T, pink curve) shows three degradation peaks at 581.88 °C, 607.54 °C and at 679.52 °C (corresponding to oxidation temperatures, Fig. 11b). These temperatures are the points of maximum weight loss. The first two peaks (weight loss of 41.90%, 3.760 mg) are not well resolved, but they are better resolved than in the Run 051218. This first peak starts at 531.07 °C (extrapolated onset T). The third degradation peak starts at 652.71 °C (non-extrapolated onset T, Fig. 10b), with a DTA peak at 679.52 °C and a weight loss of 4.935% (0.4427 mg, Fig. 11a). The degradation process is not complete at 850 °C, with a residual mass of 53.21% (4.774 mg, Fig. 11b), being the total weight loss of the process of 46.79% (4.198 mg, Fig. 11b). These results seem similar to the results under an air atmosphere of the work [8]. The comparison between both runs gives similar results (in the range of the reproducibility results of the standard sample). The differences could be explained by different particle size of both samples, different sample amount and due to the TGA furnace internal variability, among other factors.

4. Conclusion

As a result of the work carried out, the optimal conditions for the synthesis of carbon nanotubes by CCVD from propan-butan mixture were determined.

In this study multi walled carbon nanotubes were synthesized by a CCVD method, using catalysts consisting of Ni particles supported on the naturally occurring minerals diatomite and shungite. In Raman spectra of CNTs the intensity ratio $I_{(G)}/I_{(D)}$ for 650 °C is higher than that for 700 °C and then it begins to increase with increasing temperature.

Thus, there is a switch point at 700 °C when the “low” defect density regime became valid. SEM images of samples show that diameter of CNTs which were synthesized on the surface of diatomite/shungite samples were in the range of 33–100.3 nm.

Acknowledgments

This research was funded by the Science Committee of the Ministry of Education and Science of the Republic of Kazakhstan (Grant No. 08856321) “Obtaining fiber composite materials by electrospinning and creating electrodes based on them for supercapacitors” and by EMLab of University of Reading, Reading, UK).

Electron microscopy was carried out at Reading by Dr Peter Harris. The TGA analysis was also conducted at Reading by Dr. Pedro Rivas-Ruiz (CAF technician), under the supervision of the academic leader Dr. Hisham Al Obaidi.

References

- [1]. S. Iijima, *Nature* 354 (1991) 56–58. DOI: [10.1038/354056a0](https://doi.org/10.1038/354056a0)
- [2]. T. Guo, P. Nikolaev, A. G. Rinzler, D. Tomanek, D.T. Colbert, R.E. Smalley, *J. Phys. Chem.* 99 (1995) 10694–10697. DOI: [10.1021/j100027a002](https://doi.org/10.1021/j100027a002)
- [3]. M. Endo, K. Takeuchi, S. Igarashi, K. Kobori, M. Shiraishi, H. W. Kroto, *J. Phys. Chem. Solids* 54 (1993) 1841–1848. DOI: [10.1016/0022-3697\(93\)90297-5](https://doi.org/10.1016/0022-3697(93)90297-5)
- [4]. N. Yahya, *Carbon and Oxide Nanostructures: Synthesis, Characterisation and Applications*, Springer Science & Business Media, 2011.
- [5]. X.D. Yang, *J. Alloy. Compd.* 563 (2013) 216–220. DOI: [10.1016/j.jallcom.2013.02.066](https://doi.org/10.1016/j.jallcom.2013.02.066)
- [6]. M. Endo, T. Hayashi, Y. Ahm Kim, M. Terrones, M.S. Dresselhaus, *Philos. Trans. R. Soc. Lond.*

- A Math. Phys. Eng. Sci.* 362 (2004) 2223–2238. DOI: [10.1098/rsta.2004.1437](https://doi.org/10.1098/rsta.2004.1437)
- [7]. N. Saito, Y. Usui, K. Aoki, N. Narita, M. Shimizu, K. Hara, N. Ogiwara, K. Nakamura, N. Ishigaki, H. Kato, S. Taruta, M. Endo, *Chem. Soc. Rev.* 38 (2009) 1897–1903. DOI: [10.1039/B804822N](https://doi.org/10.1039/B804822N)
- [8]. Y. Shimizu, S. Miki, T. Soga, I. Itoh, H. Todoroki, T. Hosono, K. Sakaki, T. Hayashi, Y.A. Kim, M. Endo, S. Morimoto, A. Koide, *Scr. Mater.* 58 (2008) 267–270. DOI: [10.1016/j.scriptamat.2007.10.014](https://doi.org/10.1016/j.scriptamat.2007.10.014)
- [9]. K. Fujisawa, H.J. Kim, S.H. Go, H. Muramatsu, T. Hayashi, M. Endo, T.C. Hirschmann, M.S. Dresselhaus, Y.A. Kim, P.T. Arauj, *Appl. Sci.* 6 (2016) 109. DOI: [10.3390/app6040109](https://doi.org/10.3390/app6040109)
- [10]. M. Fujishige, W. Wongwiriyan, H. Muramatsu, K. Takeuchi, S. Arai, *J. Phys. Chem. Solids* 113 (2018) 229–234. DOI: [10.1016/j.jpcs.2017.10.010](https://doi.org/10.1016/j.jpcs.2017.10.010)
- [11]. O.K. Park, H. Choi, H. Jeong, Y. Jung, J. Yu, J.K. Lee, J.Y. Hwang, S.M. Kim; Y. Jeong, C.R. Park, M. Endo, B.C. Ku, *Carbon* 118 (2017) 413–421. DOI: [10.1016/j.carbon.2017.03.079](https://doi.org/10.1016/j.carbon.2017.03.079)
- [12]. N. Kobayashi, Y. Inden, M. Endo, *J. Power Sources* 326 (2016) 235–241. DOI: [10.1016/j.jpowsour.2016.06.117](https://doi.org/10.1016/j.jpowsour.2016.06.117)
- [13]. J.C. García-Gallegos, I. Martín-Gullón, J.A. Conesa, Y.I. Vega-Cantú, F.J. Rodríguez-Macías, *Nanotechnology* 27 (2016) 015501. DOI: [10.1088/0957-4484/27/1/015501](https://doi.org/10.1088/0957-4484/27/1/015501)
- [14]. R.A. DiLeo, B.J. Landi, R.P. Raffaele, *J. Appl. Phys.* 101 (2007) 064307. DOI: [10.1063/1.2712152](https://doi.org/10.1063/1.2712152)
- [15]. L.G. Cançado, A. Jorio, E.H. Martins Ferreira, F. Stavale, C.A. Achete, R.B. Capaz, M.V.O. Moutinho, A. Lombardo, T.S. Kulmala, A.C. Ferrari, *Nano Lett.* 11 (2011) 3190–3196. DOI: [10.1021/nl201432g](https://doi.org/10.1021/nl201432g)
- [16]. M.M. Lucchese, F. Stavale, E.H. Martins Ferreira, C. Vilani, M.V.O. Moutinho, R.B. Capaz, C.A. Achete, A. Jorio, *Carbon* 48 (2010) 1592–1597. DOI: [10.1016/j.carbon.2009.12.057](https://doi.org/10.1016/j.carbon.2009.12.057)
- [17]. R. Saito, A. Grüneis, Ge.G. Samsonidze, V.W. Brar, G. Dresselhaus, M.S. Dresselhaus, A. Jorio, L.G. Cançado, C. Fantini, M.A. Pimenta, *New J. Phys.* 5 (2003) 157. DOI: [10.1088/1367-2630/5/1/157](https://doi.org/10.1088/1367-2630/5/1/157)
- [18]. H. Nii, Y. Sumiyama, H. Nakagawa, A. Kunishige, *Appl. Phys. Express* 1 (2008) 064005. DOI: [10.1143/APEX.1.064005](https://doi.org/10.1143/APEX.1.064005)
- [19]. Y.-C. Hsieh, Y.-C. Chou, C.-P. Lin, T.-F. Hsieh, C.-M. Shu, *Aerosol Air Qual. Res.* 10 (2010). DOI: [10.4209/aaqr.2009.08.0053](https://doi.org/10.4209/aaqr.2009.08.0053)